

Article

Synthesis of SAPO-34 Molecular Sieves via Novel Intermittent Hydrothermal Treatment and Its Effect on the Crystallization and Product Properties

Zhihui Guo ^{1,2}, Ping Miao ^{1,*}, Weiping Zhu ^{1,*}, Lei Guo ¹, Fei Li ¹, Yunpeng Xue ¹, Qi Yin ¹, Ruixue Yuan ² and Lianbin Xu ^{2,*}

¹ Applied Catalysis Department, National Institute of Clean-and-Low-Carbon Energy, Beijing 102209, China; guozhihui@nicenergy.com (Z.G.); guolei@nicenergy.com (L.G.); lifei@nicenergy.com (F.L.); xueyunpeng@nicenergy.com (Y.X.); yinqi@nicenergy.com (Q.Y.)

² State Key Laboratory of Organic-Inorganic Composites, Beijing University of Chemical Technology, Beijing 100029, China; yuanrx@mail.buct.edu.cn

* Correspondence: miaoping@nicenergy.com (P.M.); zhuweiping@nicenergy.com (W.Z.); xulb@mail.buct.edu.cn (L.X.); Tel.: +86-10-57339895 (P.M.); +86-10-57339357 (W.Z.); +86-10-64449241 (L.X.)

Academic Editors: Benoît Louis, Qiang Wang and Marcelo Maciel Pereira

Received: 13 March 2017; Accepted: 26 April 2017; Published: 11 May 2017

Abstract: Intermittent hydrothermal treatment was introduced into the synthesis of SAPO-34 molecular sieves to control the nucleation and the growth in the crystallization. The effect of the crystallization time, the order of long-time and short-time crystallization in two-stage crystallization, and frequency in multi-stage crystallization on synthesis, physicochemical properties and catalytic performance for conversion of methanol to light olefins (MTO) has been studied. The results show that pure SAPO-34 can be obtained with increasing crystallization time. The interruption of the initial crystallization is more beneficial for improving the Si distribution and the MTO catalytic performance of SAPO-34 molecular sieves. The sample obtained by repeatedly alternating heating and cooling during crystallization shows smaller particle size, higher acidity, longer lifetimes and higher yields of ethylene than that obtained by the conventional continuous crystallization at high temperature.

Keywords: intermittent hydrothermal treatment; SAPO-34; synthesis; MTO; catalytic performance

1. Introduction

The methanol-to-olefins (MTO) process has attracted much attention because of the increasing demand for light olefins in petrochemical industries [1]. In the MTO reaction, the SAPO-34 molecular sieve has been considered to be a uniquely effective catalyst for the conversion of methanol to olefins with high catalytic activity and selectivity, due to its appropriate small pores (0.38–0.43 nm), mild acidity, and high hydrothermal stability [2,3]. However, coke can be easily formed due to mass transport limitations and the fast and strong exothermicity of MTO reaction, which causes rapid deactivation. As reported by Xing et al. [4], certain content of carbon buildup can constrict the pores of SAPO-34 and benefit the product selectivity to smaller olefins. Thus, if the lifetime of SAPO-34 in a single MTO process can be increased, the residence time of SAPO-34 molecular sieve catalysts in the industrial reactor will be increased, the content of carbon buildup will be able to be easily controlled, and the selectivity of ethylene and propylene in industry will be increased. Therefore, there are various pieces of research about increasing the SAPO-34 molecular sieve lifetime in the MTO process [2,3,5–7].

It has been reported that SAPO-34 molecular sieves with different particle sizes, pore shapes, or acidities obtained by different synthesis methods or conditions show various activities, lifetimes, or selectivities in the MTO process [2,8–11]. There are some parameters, such as template [12–16], Si/Al

ratio [17–19], crystallization time [3] and temperature [2,20] that influence the synthesis and properties of the SAPO-34 molecular sieve [21,22], in which the crystallization time and temperature are very important factors, which can be easily controlled in industry. Aghaei et al. [3] studied the effects of crystallization time and temperature on physicochemical properties and catalytic performance in the MTO process. The results show that the crystallinity, morphology, particle size, surface area, purity and textural properties are affected apparently by crystallization time and temperature. The impact of crystallization temperature on particle size is much more than that of crystallization time. Dargahi et al. [20] synthesized SAPO-34 nanoparticles at a high crystallization temperature of 400 °C and short synthesis time of 45 min. They found that SAPO-34 and SAPO-5 form simultaneously in the first 30 min, then SAPO-5 phase transforms to SAPO-34 in the next 15 min, and then SAPO-34 framework degrades after 45 min at high temperature. However, it is very difficult to control the reaction at high temperature. As reported by Wang et al. [2], varying temperature can affect the particle size of SAPO-34. However, only the two-step crystallization is reported, and it is only conducted from low temperature to high. Temperature fluctuations sometimes may occur during the production of SAPO-34 in industry. It is necessary to discuss the influence of the cooling process and the repeated temperature fluctuation in the crystallization on the synthesis, properties, and catalytic performance for conversion of methanol to light olefins of SAPO-34 molecular sieve.

In this work, various SAPO-34 molecular sieves were synthesized via intermittent crystallization in the hydrothermal treatment. The synthesized SAPO-34 molecular sieves were characterized by X-ray powder diffraction (XRD), scanning electron microscopy (SEM), Brunauer-Emmett-Teller method (BET), X-ray fluorescence (XRF), nuclear magnetic resonance (NMR), temperature-programmed desorption of ammonia adsorbed (NH₃-TPD), and particle size distribution analysis. Then, the MTO reaction over the SAPO-34 catalysts was performed. The lifetime and product selectivity were studied in detail. These studies were expected to deepen the understanding of the influence of the heating and cooling alternating crystallization on the nucleation and the growth in the crystallization. Moreover, it will also provide an easy and effective method to obtain SAPO-34 molecular sieves with good properties in MTO processes.

2. Results and Discussion

2.1. Influence of Total Crystallization Time on the Yields, Purity and Average Particle Size

The crystallinity, particle size and purity of SAPO-34 can be affected, apparently, by crystallization time [3,23]. SAPO-34s were synthesized with different crystallization times. Table 1 shows that the yield increases as the crystallization time increases. It increases slowly after 16 h, which indicates that the reaction has been fully carried out after 16 h. The yields are a little low for the SAPO-34 synthesis. The possible reason is that the solid content of the gel is a little low for improving the heat transfer. The mass transfer is inhibited with the consumption of the raw material in the static reactor. Besides, the reactor, reaction condition, as well as repeated washing can also cause the low yields. Many methods, like adjusting the recipes, adding an agitator in the crystallization, and hydrothermally treating at higher temperature, are being considered to increase the yields recently.

Table 1. Yields, relative content of SAPO-34, and the average particle size of the samples.

Sample	Yield (%)	The Relative Content of SAPO-34 in the Crystals (%)	Particle Size (μm)	
			D(50)	SEM
S(4)	0.11	81.4	-	-
S(8)	2.88	99.9	-	-
S(12)	12.50	100	8.92	8.10
S(16)	23.07	100	10.70	9.38
S(24)	28.05	100	12.70	11.76

The XRD patterns of the synthesized samples are given in Figure 1. It can be seen that all the samples are in agreement with that of the CHA-structure SAPO-34 (PDF 47-0617) [2]. However, a little impurity can be seen in the S(4) and S(8) samples (peaks at $2\theta = 7.4^\circ$ and 22.4°), which may be the aluminum phosphate carbon hydrogen nitride (PDF 89-8244), SAPO-5 (PDF 49-0659) or their mixture [22,23]. Because of the same space group and the low concentration, it is difficult to distinguish between them in the XRD patterns. Further research is needed in future. The relative content of SAPO-34 in the crystals is obtained roughly, as shown in Table 1. It increases with increasing crystallization time. Thus, pure SAPO-34 can be obtained as the crystallization time increases to 12 h. Table 1 also lists the average particle size of the samples (D(50)). It increases with increasing crystallization time because of the growth of crystals in the continuous crystallization. However, several experiments show that the average particle size of the samples obtained with short crystallization times under the same reaction conditions always varies from 5 to 9 μm for S(4) and from 8 to 15 μm for S(8). The possible reason is that very few crystal nuclei are produced at the beginning of the crystallization. The particle aggregation and growth take place rapidly after nucleation [22] because of the high concentration of material and the fast mass transfer rate. Thus, a few large crystals with some defects preliminarily appear, which are easily shattered and dissolved. Besides, the amorphous phase may wrap around the crystals. It is difficult to control the particle size of SAPO-34 only by shortening crystallization time. Therefore, the total crystallization time at 200 $^\circ\text{C}$ should be longer than 12 h. The particle size from SEM is a little smaller than that from the Malvern mastersizer because of the different measuring principle. The data from SEM via the rough statistics of 120–220 particles are the cube's edges of SAPO-34s, but that from Malvern mastersizer are the statistically-equivalent volume diameters of a larger number of particles. However, the data from both methods show similar variation that can support the conclusion.

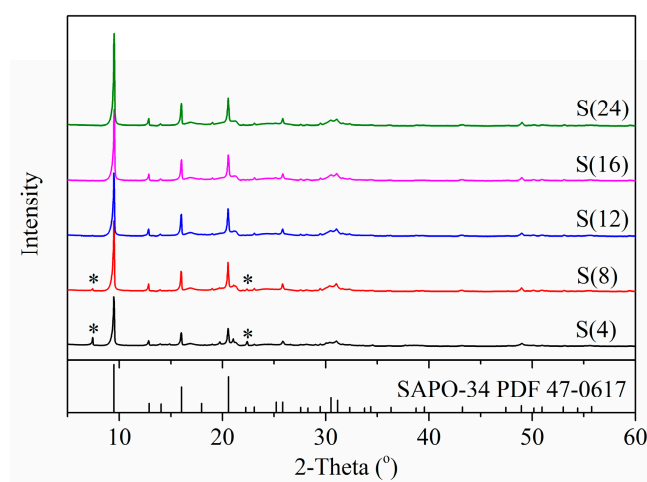


Figure 1. XRD (X-ray powder diffraction) patterns of samples synthesized with different crystallization time. S(4), 4 h; S(8), 8 h; S(12), 12 h; S(16), 16 h; S(24), 24 h.

2.2. Two-Stage Crystallization

Two-stage heating and cooling alternating crystallization was introduced into the hydrothermal treatment. In the crystallization, the balance of the system is broken by the temperature fluctuation, which might affect the nucleation and the growth of the crystals. The growth can only take place after nucleation, and the composition of the newly-grown layer would be different from that of the original layer with the growth of the crystal [18]. Thus, the distribution of the crystallization time by the alternation of heating and cooling could affect the nucleation, growth, composition, and properties of the crystals. Samples (S(4-12) and S(12-4)) were synthesized in the opposite crystallization order to study the effect of the order of long-time and short-time crystallization in the two-stage crystallization

on the properties of SAPO-34. As shown in Table 2, the yields and the elemental composition of the samples are similar. The D(50) of S(4-12) is a little smaller than S(12-4) and S(16), while the acidity of S(4-12) is a little larger (Table 2 and Figure S1). The MTO catalytic performances of the samples are investigated at 450 °C and 3 h⁻¹ WHSV. S(4-12) shows relatively lower deactivation with the methanol conversion dropping below 85% and higher yield of ethylene plus propylene than the others (Figures 2 and 3). As reported by Liu et al. [18], the Si-concentration in the SAPO-34 crystals increases from the core to the surface because the properties of the mixture solution (pH value, reactant species and concentrations) change. Several kinds of crystals with different Si distribution can be produced in the hydrothermal process. In the two-stage crystallization, the particle size, Si distribution in the crystals, and properties of the mixture solutions are different after the first stage crystallization with different crystallization time. Since the equilibrium of the growth and second nucleation is broken by the interruption of the crystallization, the Si distribution in the crystals changes in different crystallization environments. As a result, the acidity and the MTO performance of the products are changed. After long-time crystallization of the first stage, the crystals are stable and the concentration of the Si, Al, and P in the mixture solution is low. The interruption has little effect on the nucleation and growth, so the particle size, composition, and properties of S(12-4) and S(16) are similar. Therefore, short-time crystallization of the first stage is beneficial for improving the Si distribution and the MTO catalytic performance of the SAPO-34 molecular sieves.

Table 2. Yields and the average particle size of the samples.

Sample	Yield (%)	Particle Size (μm)		Elemental Composition (mol %)	Total Acidity (mmol NH ₃ /g)	Strong Acid ¹ (mmol NH ₃ /g)	Weak Acid ² (mmol NH ₃ /g)
		D(50)	SEM				
S(4-12)	24.04	9.70	8.38	Si _{0.085} Al _{0.474} P _{0.441}	1.48	0.86	0.62
S(12-4)	23.83	10.20	8.80	Si _{0.083} Al _{0.475} P _{0.442}	1.28	0.76	0.52
S(16)	23.07	10.70	9.38	Si _{0.086} Al _{0.472} P _{0.442}	1.24	0.73	0.51

¹ desorption peaks of ammonia centered around 350–400 °C; ² desorption peaks of ammonia centered around 150–200 °C.

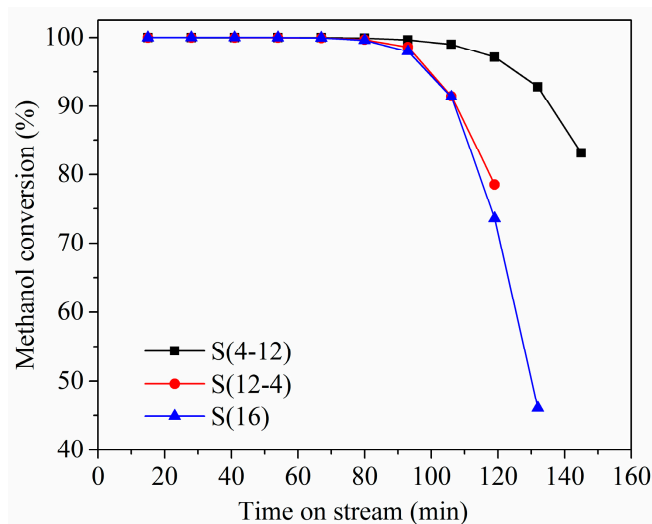


Figure 2. Methanol conversions in the MTO (methanol-to-olefins) reaction on the S(4-12), S(12-4) and S(16) samples. Reaction conditions: $T = 450$ °C, WHSV = 3 h⁻¹, 95 wt % methanol solution, sample weight = 0.2 g.

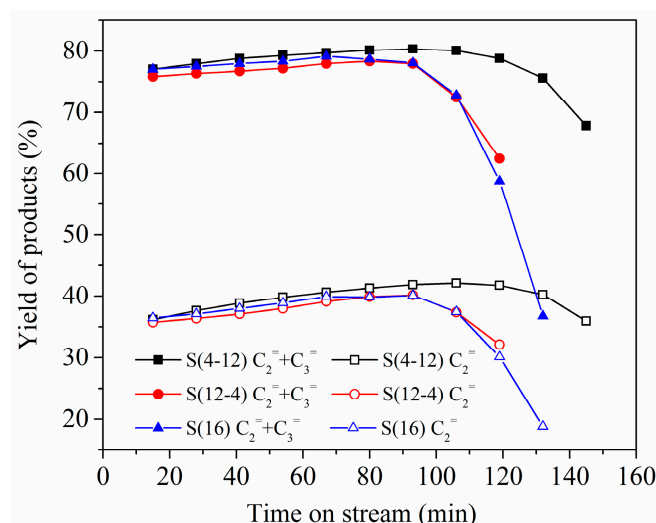


Figure 3. Product distribution curves in the MTO reaction over S(4-12), S(12-4) and S(16) samples. Reaction conditions: $T = 450\text{ }^{\circ}\text{C}$, $\text{WHSV} = 3\text{ h}^{-1}$, 95 wt % methanol solution, sample weight = 0.2 g.

2.3. Multi-Stage Crystallization

The distribution of the crystallization time in the intermittent hydrothermal treatment can also be adjusted by changing the frequency. At the same total crystallization time and the priority of short time in the initial stage of crystallization, samples S(4-4-4-4), S(4-4-8), S(4-12) and S(16) are synthesized at various crystallization cycles and analyzed to investigate the effect of the frequency in multi-stage crystallization on nucleation, growth, composition, and properties of SAPO-34. All the XRD patterns of the samples (Figure 4) are confirmed in agreement with that of the CHA-structure SAPO-34 (PDF 47-0617). The yields and the elemental compositions of Si, Al and P of the samples are similar, as shown in Table 3. This indicates that the crystallization time distribution of the intermittent hydrothermal treatment has very little influence on yields and elemental composition with the same total crystallization time. However, the $D(50)$ s of the samples vary according to the frequency. They increase with an increase in time of continuous crystallization at high temperature. SEM images and particle size distribution histograms of S(4-4-4-4) and S(16) are shown in Figure 5. Both samples consist of crystals with a cubical shape, whereas their particle sizes are a little different. The particle size distribution of S(4-4-4-4) is more narrow than that of S(16). The same synthetic experiments of S(4-4-4-4) and S(16) are reproduced. As shown in Table 4, the particle size of S(4-4-4-4)s synthesized at the same condition is always smaller than that of S(16)s with standard deviations (Std. Dev.) of $D(50)$ 1.62 and 1.27 μm , respectively. As reported by Xu et al. [24], the rate of crystal growth decreases faster than that of nucleation as the temperature decreases. So, in crystallization alternating heating and cooling, the temperature fluctuation has different effects on the nucleation and growth of crystals. The mass transfer is inhibited, and small crystals are perhaps difficult to dissolve and deposit on larger particles in the cooling process. Thus, the growth of crystals may be inhibited. More crystal nuclei are generated and remain stable. Therefore, the continuous crystallization at high temperature is beneficial for crystal growth, and the interruption of crystallization can restrain growth and promote nucleation. The particle sizes of the samples synthesized by alternating heating and cooling are smaller than those synthesized by the normal method. Further detailed research about the mechanism and kinetics of crystallization using alternating heating and cooling should be studied in future.

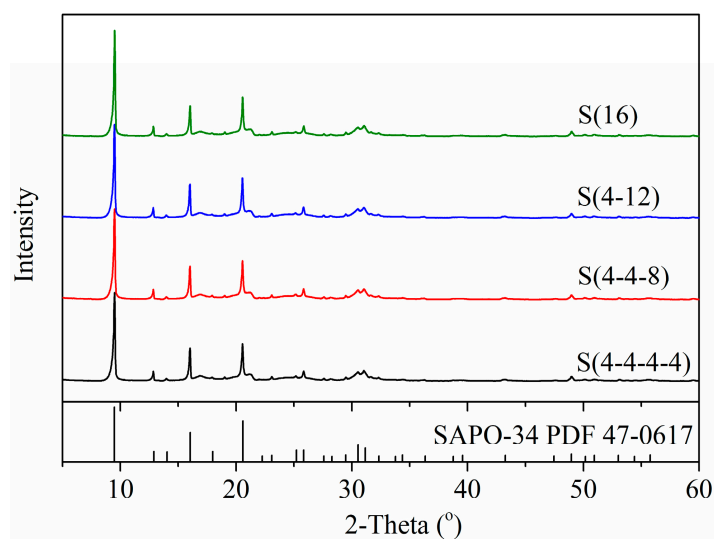


Figure 4. XRD patterns of samples synthesized with different crystallization time distribution in the multi-stage intermittent crystallization.

Table 3. Yields, the average particle size, Elemental Composition of the samples.

Sample	Yield (%)	Particle Size (μm)		Elemental Composition (mol %)	Surface Area (m^2/g)			Pore Volume (cm^3/g)		
		D(50)	SEM		S_{micro}	S_{ext}	S_{BET}	V_{micro}	V_{meso}	V_{total}
S(4-4-4-4)	22.36	6.75	5.28	$\text{Si}_{0.081}\text{Al}_{0.475}\text{P}_{0.444}$	890	15	905	0.32	0.01	0.33
S(4-4-8)	22.61	7.53	6.87	$\text{Si}_{0.085}\text{Al}_{0.474}\text{P}_{0.441}$	758	18	777	0.28	0.01	0.29
S(4-12)	24.04	9.70	8.38	$\text{Si}_{0.085}\text{Al}_{0.474}\text{P}_{0.441}$	755	6	761	0.27	0.00	0.27
S(16)	23.07	10.70	9.38	$\text{Si}_{0.086}\text{Al}_{0.472}\text{P}_{0.442}$	773	14	787	0.28	0.01	0.29

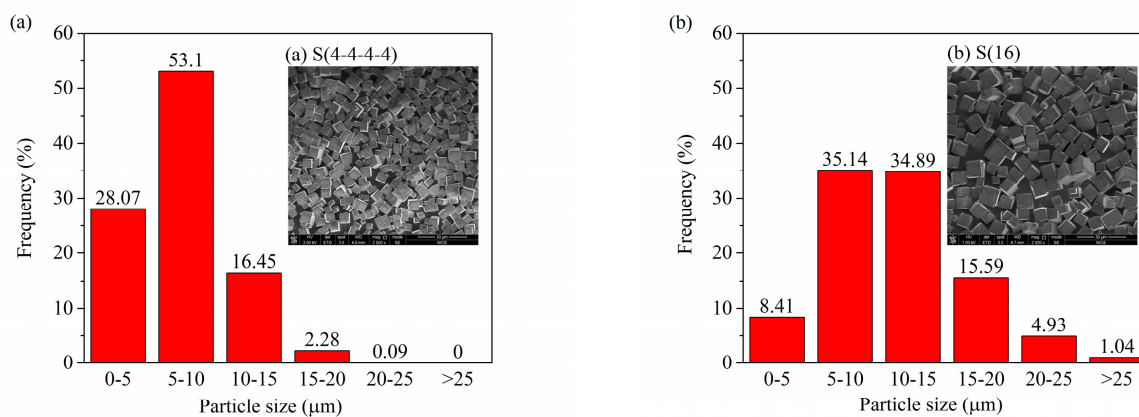


Figure 5. Particle size distribution and SEM images of SAPO-34 molecular sieve synthesized by different crystallization mode: (a) intermittent crystallization of S(4-4-4-4), the temperature of the crystallization for each 4 h is 200 °C; (b) conventional continuous crystallization for 16 h at 200 °C of S(16).

Table 4. Yields and the average particle size of the samples S(4-4-4-4) and S(16) synthesized at the same condition three times respectively.

Sample	Serial Number	Yield (%)	Particle Size (μm)	
			D(50)	SEM
S(4-4-4-4)	1	22.36	6.75	5.28
	2	26.99	3.53	2.30
	3	20.91	5.36	4.01
	Std. Dev.	3.18	1.62	1.50
S(16)	1	23.07	10.70	9.38
	2	22.99	13.20	11.96
	3	26.83	12.30	10.88
	Std. Dev.	2.19	1.27	1.30

Since the growth of crystals is inhibited, the intermittent crystallization process with Si distribution in the crystals is different from the continuous crystallization process [18]. A larger number of small crystals with uniform Si concentration are produced with intermittent crystallization. The acidity of the samples was measured by NH_3 -TPD. All the samples have two similar desorption peaks in 150–200 °C and 350–400 °C due to the low and high temperatures of desorption, respectively (Figure S2). Niwa et al. [25] reported that the temperature of the peak maximum is affected by not only the strength of acidity, but also the W/F (where W and F are the weight of samples and flow rate of carrier gas, respectively). With the same W/F in the measurement of one sample, the low temperature desorption peak of ammonia is attributed to the relatively weak acidity (Table 5) that is attributed to the hydroxyl groups bonded to the defect sites (POH, SiOH, and AlOH). The high temperature desorption peak of ammonia is attributed to the relatively strong acidity (Table 5) due to the bridging hydroxyl group of the strong Brønsted acid site [4]. The total acidity of S(4-4-4-4) and S(4-4-8) is greater than the others (Table 5). Solid-state ^{29}Si , ^{27}Al , and ^{31}P MAS NMR spectra are obtained to investigate the structural configuration and the local atomic environments of the samples. As shown in Figure 6a, the ^{29}Si spectra of the samples show an obvious peak at -90 or -89 ppm due to Si(O₄Al) species. This suggests that the majority of the Si enters the framework via the SM II mechanism, in which silicon atoms are substituted for phosphorus atoms [26]. The weak peak near -94 and -97 ppm can be ascribed to Si(1Si, 3Al) and Si(2Si, 2Al) species, respectively. There are some shoulder peaks between -76 and -87 ppm in the spectra of S(4-12) and S(16), which should arise from Si(O₄Al), Si(O₃Al), Si(O₂Al) or Si(1Si, 1Al) species [27,28]. The appearance of multiple silicon environments illustrates that two silicon atoms being substituted for a pair of phosphorus and aluminum atoms via the SM III mechanism probably occurs synergistically with the SM II mechanism [26]. Two peaks near -12 and 40 ppm are observed in the ^{27}Al spectra (Figure 6b). The peak at -12 ppm can be attributed to the hexa-coordinated Al species, which is formed by additional interactions of water with the framework aluminum [5,28]. The other peak at 37 or 40 ppm is attributed to tetrahedral Al. As reported by Shen et al. [9], the Si atoms in the second coordination sphere of Al, relative to P atoms, can shift the ^{27}Al peak to a lower field. Thus, in the samples of S(4-12) and S(16), the content of Si in the second coordination sphere of Al is a little larger than that in the samples of S(4-4-4-4) and S(4-4-8). The ^{31}P NMR spectra are shown in Figure 6c. The strong resonance peak at -29 or -27 ppm is the predominant tetrahedral P(OAl)₄ environment in the framework. The broad peak around -19 ppm in the spectra of S(4-12) and S(16) can be attributed to P atoms coordinated with water molecules in the form of species P(OAl)_(4-x)(OH)_x [29,30]. The ^{29}Si , ^{27}Al , and ^{31}P MAS NMR results show that the samples S(16) and S(4-12) present more defects than the others. Fjermestad et al. [31] reported that the Si/Al exchange (the SM III mechanism), and the generation of H₃PO₄ from P atoms in the defects present in the materials may form Si islands. Thus, because of the uniform Si concentration and lower number of defects in S(4-4-4-4), Si island formation may be inhibited.

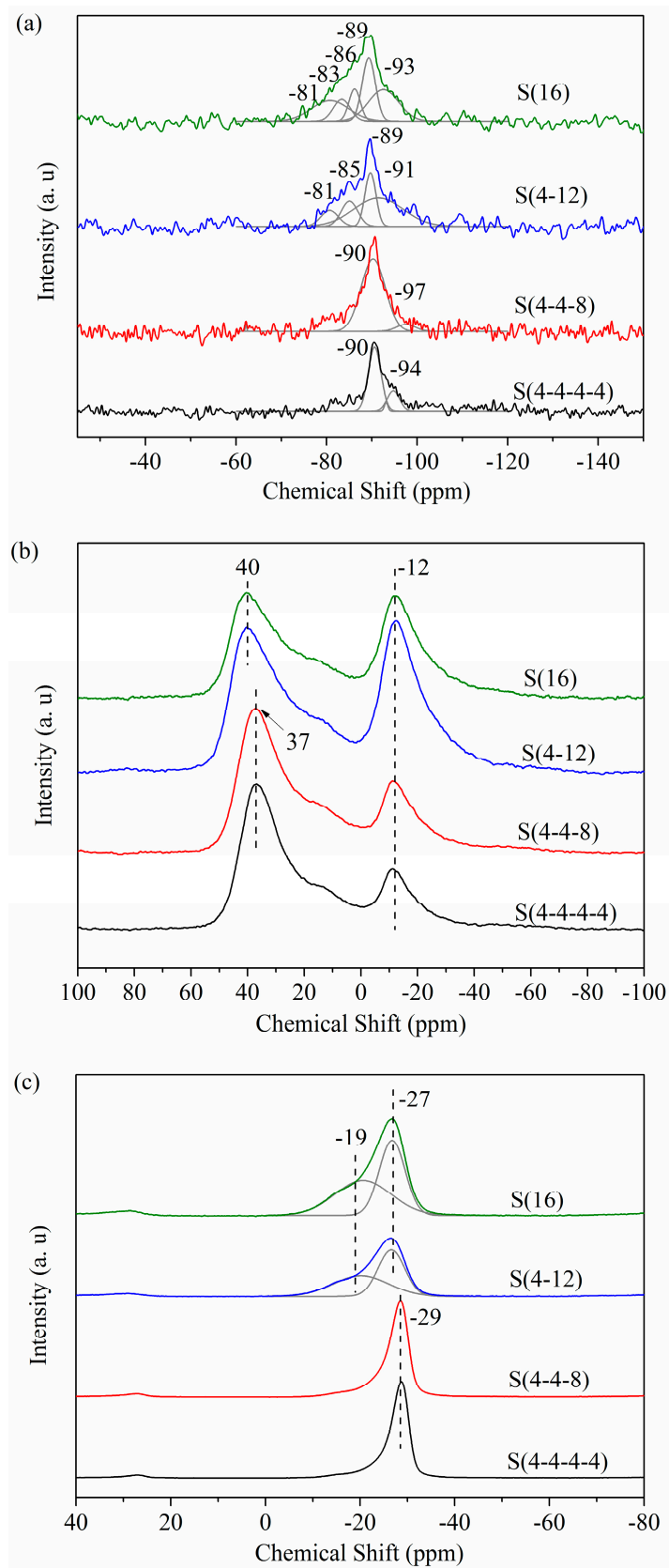


Figure 6. Solid-state (a) ^{29}Si ; (b) ^{27}Al ; (c) ^{31}P MAS NMR spectra of samples synthesized with different crystallization time distribution in the multi-stage intermittent crystallization.

Table 5. NH₃-TPD of the samples synthesized with different crystallization time distribution.

Sample	Total Acidity (mmol NH ₃ /g)	Strong Acid ¹ (mmol NH ₃ /g)	Weak Acid ² (mmol NH ₃ /g)
S(4-4-4-4)	1.75	1.03	0.72
S(4-4-8)	1.73	0.99	0.74
S(4-12)	1.48	0.86	0.62
S(16)	1.24	0.73	0.51

¹ desorption peaks of ammonia centered around 350–400 °C; ² desorption peaks of ammonia centered around 150–200 °C.

The MTO catalytic performances of the samples S(4-4-4-4), S(4-4-8), S(4-12), and S(16) are investigated at 450 °C and 3 h⁻¹ WHSV. After the methanol conversion below 99%, more financial and technological resources should be devoted to purifying and separating products in the MTO industry. Thus, we define the duration of the methanol conversion over 99% as the lifetime. As shown in Figure 7, methanol conversion over 99% could be maintained for 132.4, 106.1, 105.8, and 84.7 min for S(4-4-4-4), S(4-4-8), S(4-12), and S(16), respectively. The greater extension of MTO catalytic lifetime of S(4-4-4-4) is probably due to the smaller particle size, and the relatively uniform Si distribution of the crystals [32]. However, the deactivation rate of S(4-4-8) is a little faster than that of S(4-12) after the methanol conversion lower than 99%. It is probably caused by the different distribution of Si and pore in the structure and the higher weak acidity of S(4-4-8), which will affect the coke types and the deposition rate. Further detailed research is being undertaken. The yields of ethylene plus propylene in the MTO reaction for all the samples are between 76% and 81% under >99% methanol conversion, while the yields of ethylene for S(4-4-4-4) and S(4-4-8) are higher than that for S(4-12) and S(16) (Figure 8). It can be deduced that the stronger acidity is more beneficial for the selectivity of ethylene. As reported by Li et al. [33], the ratio of ethylene to propylene is not controlled by a faster diffusion of ethylene versus propylene, but is affected by differences in acid strength, and that this different acidity is due to a different distribution of silicon. Thus, the existence of defective sites at −76 to −87 ppm in ²⁹Si NMR spectra (Figure 6a) may decrease the acid strength and decrease the ratio of ethylene to propylene. Moreover, the yields of ethylene for the samples increase with the reaction time at high methanol conversion and accompanied by the gradual decrease of propylene. As reported by Li et al. [29], the selectivity of olefins is strongly affected by thermodynamic distribution at high methanol conversion, and is also affected by the transition states. With the longer lifetime of S(4-4-4-4), the coke level can be controlled more easily to approach optimized product selectivity.

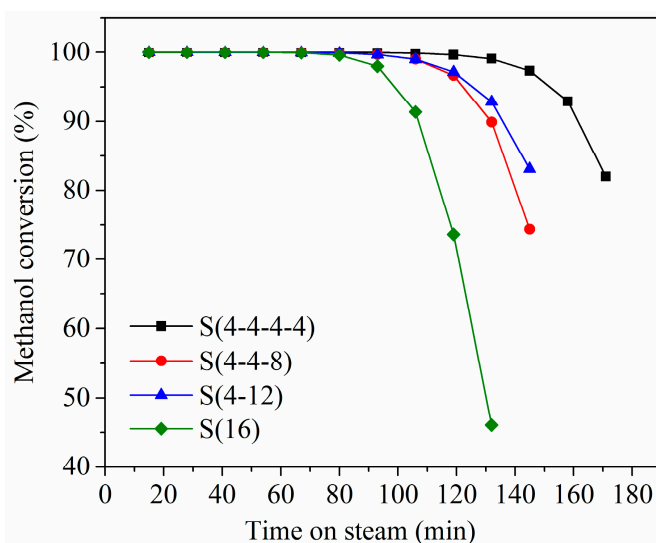


Figure 7. Methanol conversions in the MTO reaction on the SAPO-34 samples. Reaction conditions: $T = 450$ °C, WHSV = 3 h⁻¹, 95 wt % methanol solution, sample weight = 0.2 g.

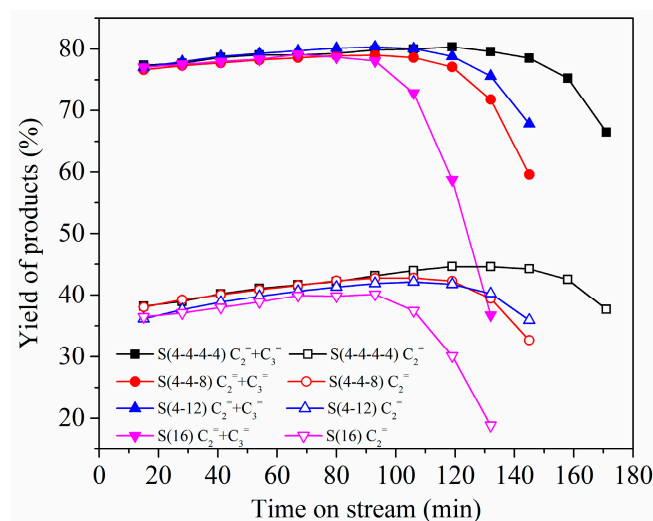


Figure 8. Yields of C_2H_4 and C_2H_4 plus C_3H_6 in the MTO reaction on the SAPO-34 samples. Reaction conditions: $T = 450\text{ }^\circ\text{C}$, $WHSV = 3\text{ h}^{-1}$, 95 wt % methanol solution, sample weight = 0.2 g.

3. Materials and Methods

3.1. Synthesis of SAPO-34 Molecular Sieves

SAPO-34 molecular sieves were synthesized by hydrothermal methods at different temperature control modes. Pseudoboehmite (70 wt %, Al_2O_3), phosphoric acid (85 wt %), silica sol (30 wt %) were used as the sources of the framework elements. Triethylamine (TEA) was used as structure directing agent (SDA). In a typical synthesis, pseudoboehmite, phosphoric acid, and H_2O were mixed and stirred for about 1 h. Then, TEA was added to the solution. After stirring continuously for another 0.5 h, silica sol was added to the precursor solution. The composition of the gel was $1Al_2O_3:1P_2O_5:0.6SiO_2:60H_2O:3TEA$. The final resulting gel was stirred for another 2 h, and then aged for 2 h. Then, the homogeneous gel was transferred into a Teflon lined stainless steel autoclave and hydrothermally treated in a furnace by different processes as follows:

S(4-4-4-4) crystallization was first conducted at $200\text{ }^\circ\text{C}$ for 4 h, then the reactor was cooled naturally. After 1 h (the temperature was about $45\text{ }^\circ\text{C}$), the reactor was put into a furnace of $200\text{ }^\circ\text{C}$ for another 4 h. The above hydrothermal treatment was conducted for four cycles.

The other samples (S(4-4-8), S(4-12), S(12-4), S(16), S(12), S(8), and S(4)) were prepared as in the above procedure of preparing S(4-4-4-4) except that the hydrothermal treatments were conducted for different cycles and different hydrothermal times at $200\text{ }^\circ\text{C}$. For example, for S(4-4-8), the hydrothermal treatments were conducted for three cycles and the hydrothermal times at $200\text{ }^\circ\text{C}$ of the three cycles were 4 h, 4 h, and 8 h in sequence. For S(16), S(12), S(8), and S(4), the samples were hydrothermally treated at $200\text{ }^\circ\text{C}$ for 16 h, 12 h, 8 h and 4 h, respectively.

After the above hydrothermal treatment, the solid products were collected by centrifugation and washed 4–6 times with deionized water. Then, as-synthesized products were dried at $110\text{ }^\circ\text{C}$ and calcined at $650\text{ }^\circ\text{C}$ for 5 h.

The yields of the products before calcination were calculated by the following equation:

$$\text{Yield} = m_s / (m_{Al_2O_3} + m_{P_2O_5} + m_{SiO_2}) \times 100\% \quad (1)$$

where m_s , $m_{Al_2O_3}$, $m_{P_2O_5}$, and m_{SiO_2} stand for the weight of the products before calcination and the dry mass of inorganic oxides in the raw material, respectively.

3.2. Characterization

The particle size of SAPO-34s was determined by Mastersizer 3000 (Malvern Instruments Ltd., Malvern, UK) using laser diffraction technique with deionized water as dispersant under ultrasonic. The particle refractive index and absorption index were 1.520 and 0.100, respectively. The crystalline structure of the products before calcination was analyzed by powder X-ray diffraction (XRD) on a Bruker D8A (Bruker AXS GmbH, Karlsruhe, Germany) with monochromatic Cu $K\alpha_1$ radiation ($\lambda = 1.5406$). The relative content of SAPO-34 in the crystals was calculated by the Equation (2):

$$\text{Content} = S_{\text{SAPO-34}}/S_{\text{All}} \quad (2)$$

where $S_{\text{SAPO-34}}$ and S_{All} are the areas of SAPO-34 peaks and all peaks in the XRD patterns, respectively.

The chemical composition of the sample was determined by X-ray fluorescence (XRF) on a XRF-ZSX Primus II spectrometer (Rigaku Co., The Woodlands, TX, USA). SEM photographs were obtained on a FEI Nova NanoSEM 450 scanning electron microscopy (FEI Co., Hillsboro, OR, USA). The BET surface areas of the samples were determined by N_2 adsorption-desorption method at -196 °C on a Micromeritics ASAP2460 surface area and pore size analyzer (Micromeritics Instrument Co., Norcross, GA, USA). The samples were degassed at 350 °C for 12 h.

The solid-state magic-angle-spinning (MAS) NMR spectra were recorded with Bruker AVANCE III 400 (89 mm bore) spectrometer (Bruker AXS GmbH, Karlsruhe, Germany) operating at 9.397 T field strength using 4 mm o.d. ZrO_2 rotors with a rotation speed of 5 KHz for ^{29}Si MAS NMR, 9 KHz for ^{27}Al MAS NMR, and 9 KHz for ^{31}P MAS NMR. Single-pulse ^{29}Si , ^{27}Al , and ^{31}P MAS NMR spectra of the samples were measured with relaxation time of 100, 2, and 5 s, respectively. The chemical shift of ^{29}Si , ^{27}Al , and ^{31}P was externally referenced to Kaolinite, $\text{Al}(\text{NO}_3)_3$ aqueous solution, 1 mol/L, and $\text{NH}_4\text{H}_2\text{PO}_4$ (ADP), respectively.

The acidity of the samples was also studied by NH_3 temperature programmed desorption (NH_3 -TPD) on an Autochem II 2920 TPD analyzer (Micromeritics Instrument Co., Norcross, GA, USA). 0.1–0.2 g sample was first pretreated at 550 °C for 30 min in He flow to remove adsorbed water. Subsequently, the sample was cooled to 100 °C and maintained for 30 min. Then NH_3 (10%, He) was adsorbed to the sample for 60 min, followed by a flow of He for 20 min. The NH_3 desorption from the samples was detected while the samples were heated from 100 °C to 600 °C at 10 °C/min.

3.3. Catalytic Activity Evaluation

The samples were pressed to slice, crushed and sieved into 0.4–0.8 μm particle size. 0.2 g samples were mixed with 0.6 g quartz and then introduced into a fixed-bed micro-reactor. Prior to reaction, the samples were conditioned at 450 °C for 1 h using N_2 flow. Then 95% methanol, preheated at 280 °C, was introduced into the reactor with a weight hourly space velocity (WHSV) of 3 h^{-1} . The tests were performed at atmospheric pressure. The products were analyzed by an on-line gas chromatograph (Agilent GC 7890A) (Agilent Technologies, Santa Clara, CA, USA) equipped with flame ionization (FID) and thermal conductivity (TCD) detectors.

4. Conclusions

In the present work, SAPO-34 molecular sieves were synthesized via intermittent crystallization in the hydrothermal treatment. The impurity phase disappears and the yield of SAPO-34 increases by increasing the crystallization time. The interruption in crystallization can restrain the growth and promote the nucleation. The average particle size of the crystals can be decreased, while the elemental composition cannot be changed. The interruption of the initial crystallization is more beneficial for improving the Si distribution and the MTO catalytic performance of the SAPO-34 molecular sieves. The particles synthesized by crystallization with frequent alternation of heating and cooling without the defective structures of $\text{Si}(0\text{Si}, 3\text{Al})$, $\text{Si}(0\text{Si}, 2\text{Al})$, $\text{Si}(1\text{Si}, 1\text{Al})$, and $\text{P}(\text{OAl})_{(4-x)}(\text{OH})_x$ show greater acidity, longer catalytic lifetimes, and higher yields of ethylene. Although the effects are visible, the

average particle size of the samples is still controlled in micrometer scale. Some suitable methods like adjusting the recipes and the reaction conditions combined with the intermittent crystallization are expected to be developed for obtaining SAPO-34 molecular sieves with smaller particle size and better properties. Besides, further research is needed to explore the effect of heating and cooling alternating crystallization on the reaction mechanism in detail.

Supplementary Materials: The following are available online at www.mdpi.com/2073-4344/7/5/150/s1, Figure S1: NH₃-TPD profiles of the samples S(4-12), S(12-4) and S(16), Figure S2: NH₃-TPD profiles of the samples synthesized with different crystallization time distribution in the multi-stage intermittent crystallization.

Acknowledgments: The authors gratefully thank Shenhua Group Corporation Ltd. for the financial support of the research (SHJT-07-08, SHJT-11-02, SHJT-12-39, and ST930014SH05) as well as all colleagues involved in the MTO process development.

Author Contributions: Zhihui Guo, Ping Miao, Weiping Zhu, and Lianbin Xu conceived and designed the experiments; Zhihui Guo and Ruixue Yuan performed the experiments, Zhihui Guo, Ruixue Yuan, and Qi Yin analyzed the data; Weiping Zhu, Lei Guo, Fei Li, Yunpeng Xue, and Qi Yin contributed to analysis and catalytic activity evaluation tools and equipment; Zhihui Guo and Weiping Zhu wrote the paper; Ping Miao, Weiping Zhu, and Lianbin Xu participated in the review of the results.

Conflicts of Interest: The authors declare no conflict of interest.

References

1. Tian, P.; Wei, Y.; Ye, M.; Liu, Z. Methanol to Olefins (MTO): From Fundamentals to Commercialization. *ACS Catal.* **2015**, *5*, 1922–1938. [[CrossRef](#)]
2. Wang, P.; Yang, D.; Hu, J.; Xu, J.A.; Lu, G. Synthesis of SAPO-34 with small and tunable crystallite size by two-step hydrothermal crystallization and its catalytic performance for MTO reaction. *Catal. Today* **2013**, *212*, 62.e1–62.e8. [[CrossRef](#)]
3. Aghaei, E.; Haghighi, M. Effect of crystallization time on properties and catalytic performance of nanostructured SAPO-34 molecular sieve synthesized at high temperatures for conversion of methanol to light olefins. *Powder Technol.* **2015**, *269*, 358–370. [[CrossRef](#)]
4. Xing, A.; Wang, L.; Shi, Y. Evolution of coke deposit and its effect on product selectivity for methanol-to-olefin reaction in fluidized bed. *Energy Fuels* **2014**, *28*, 3339–3344.
5. Wang, C.; Yang, M.; Zhang, W.; Su, X.; Xu, S.; Tian, P.; Liu, Z. Organophosphorous surfactant-assistant synthesis of SAPO-34 molecular sieve with special morphology and improved MTO performance. *RSC Adv.* **2016**, *6*, 47864–47872. [[CrossRef](#)]
6. Sun, Q.; Wang, N.; Guo, G.; Yu, J. Ultrafast synthesis of nano-sized zeolite SAPO-34 with excellent MTO catalytic performance. *Chem. Commun.* **2015**, *51*, 16397–16400. [[CrossRef](#)] [[PubMed](#)]
7. Liu, G.; Tian, P.; Xia, Q.; Liu, Z. An effective route to improve the catalytic performance of SAPO-34 in the methanol-to-olefin reaction. *J. Nat. Gas Chem.* **2012**, *21*, 431–434. [[CrossRef](#)]
8. Charghand, M.; Haghighi, M.; Saedy, S.; Aghamohammadi, S. Efficient hydrothermal synthesis of nanostructured SAPO-34 using ultrasound energy: Physicochemical characterization and catalytic performance toward methanol conversion to light olefins. *Adv. Powder Technol.* **2014**, *25*, 1728–1736. [[CrossRef](#)]
9. Shen, W.; Li, X.; Wei, Y.; Tian, P.; Deng, F.; Han, X.; Bao, X. A study of the acidity of SAPO-34 by solid-state NMR spectroscopy. *Microporous Mesoporous Mater.* **2012**, *158*, 19–25. [[CrossRef](#)]
10. Dahl, I.M.; Mostad, H.; Akporiaye, D.; Wendelbo, R. Structural and chemical influences on the MTO reaction: A comparison of chabazite and SAPO-34 as MTO catalysts. *Microporous Mesoporous Mater.* **1999**, *29*, 185–190. [[CrossRef](#)]
11. Nishiyama, N.; Kawaguchi, M.; Hirota, Y.; Van Vu, D.; Egashira, Y.; Ueyama, K. Size control of SAPO-34 crystals and their catalyst lifetime in the methanol-to-olefin reaction. *Appl. Catal. A Gen.* **2009**, *362*, 193–199. [[CrossRef](#)]
12. Álvaro-Muñoz, T.; Márquez-Álvarez, C.; Sastre, E. Use of different templates on SAPO-34 synthesis: Effect on the acidity and catalytic activity in the MTO reaction. *Catal. Today* **2012**, *179*, 27–34. [[CrossRef](#)]
13. Rimaz, S.; Halladj, R.; Askari, S. Synthesis of hierarchical SAPO-34 nano catalyst with dry gel conversion method in the presence of carbon nanotubes as a hard template. *J. Colloid Interface Sci.* **2016**, *464*, 137–146. [[CrossRef](#)] [[PubMed](#)]

14. Aghamohammadi, S.; Haghghi, M. Dual-template synthesis of nanostructured CoAPSO-34 used in methanol to olefins: Effect of template combinations on catalytic performance and coke formation. *Chem. Eng. J.* **2015**, *264*, 359–375. [[CrossRef](#)]
15. Najafi, N.; Askari, S.; Halladj, R. Hydrothermal synthesis of nanosized SAPO-34 molecular sieves by different combinations of multi templates. *Powder Technol.* **2014**, *254*, 324–330. [[CrossRef](#)]
16. Sadeghpour, P.; Haghghi, M. DEA/TEAOH templated synthesis and characterization of nanostructured NiAPSO-34 particles: Effect of single and mixed templates on catalyst properties and performance in the methanol to olefin reaction. *Particuology* **2015**, *19*, 69–81. [[CrossRef](#)]
17. Xu, L.; Du, A.; Wei, Y.; Wang, Y.; Yu, Z.; He, Y.; Zhang, X.; Liu, Z. Synthesis of SAPO-34 with only Si(4Al) species: Effect of Si contents on Si incorporation mechanism and Si coordination environment of SAPO-34. *Microporous Mesoporous Mater.* **2008**, *115*, 332–337. [[CrossRef](#)]
18. Liu, G.; Tian, P.; Zhang, Y.; Li, J.; Xu, L.; Meng, S.; Liu, Z. Synthesis of SAPO-34 templated by diethylamine: Crystallization process and Si distribution in the crystals. *Microporous Mesoporous Mater.* **2008**, *114*, 416–423. [[CrossRef](#)]
19. Wu, X.C.; Anthony, R.G. Effect of feed composition on methanol conversion to light olefins over SAPO-34. *Appl. Catal. A Gen.* **2001**, *218*, 241–250. [[CrossRef](#)]
20. Dargahi, M.; Kazemian, H.; Soltanieh, M.; Rohani, S.; Hosseinpour, M. Rapid high-temperature synthesis of SAPO-34 nanoparticles. *Particuology* **2011**, *9*, 452–457. [[CrossRef](#)]
21. Askari, S.; Halladj, R.; Askari, R.; Bosari, S.S. Catalytic performance of SAPO-34 catalysts of different crystal sizes in methanol-to-olefins reactions: Effects of synthetic parameters. *Prog. React. Kinet. Mech.* **2015**, *40*, 143–153.
22. Askari, S.; Siahmard, A.B.; Halladj, R.; Alipour, S.M. Different techniques and their effective parameters in nano SAPO-34 synthesis: A review. *Powder Technol.* **2016**, *301*, 268–287. [[CrossRef](#)]
23. Valizadeh, B.; Askari, S.; Halladj, R.; Haghmoradi, A. Effect of Synthesis Conditions on Selective Formation of SAPO-5 and SAPO-34. *Synth. React. Inorg. Metal-Org. Nano-Metal Chem.* **2014**, *44*, 79–83. [[CrossRef](#)]
24. Xu, R.; Pang, W.; Huo, Q. *Chemistry-Zeolite and Porous Materials*; Science Press Ltd.: Beijing, China, 2015. (In Chinese)
25. Niwa, M.; Katada, N. Measurements of acidic property of zeolites by temperature programmed desorption of ammonia. *Catal. Surv. Asia* **1997**, *1*, 215–226. [[CrossRef](#)]
26. Prakash, A.M.; Unnikrishnan, S. Synthesis of SAPO-34: High silicon incorporation in the presence of morpholine as template. *J. Chem. Soc. Faraday Trans.* **1994**, *90*, 2291–2296. [[CrossRef](#)]
27. Zhang, L.; Bates, J.; Chen, D.; Nie, H.Y.; Huang, Y. Investigations of Formation of Molecular Sieve SAPO-34. *J. Phys. Chem. C* **2011**, *115*, 22309–22319. [[CrossRef](#)]
28. Yang, M.; Tian, P.; Wang, C.; Yuan, Y.; Yang, Y.; Xu, S.; He, Y.; Liu, Z. A top-down approach to prepare silicoaluminophosphate molecular sieve nanocrystals with improved catalytic activity. *Chem. Commun.* **2014**, *50*, 1845–1847. [[CrossRef](#)] [[PubMed](#)]
29. Li, Z.; Martínez-Triguero, J.; Concepcion, P.; Yu, J.; Corma, A. Methanol to olefins: Activity and stability of nanosized SAPO-34 molecular sieves and control of selectivity by silicon distribution. *Phys. Chem. Chem. Phys.* **2013**, *15*, 14670–14680. [[CrossRef](#)] [[PubMed](#)]
30. Zhang, Y.; Deng, Z.; Zhu, K.; Zhou, X.G. Insights into the growth of small-sized SAPO-34 crystals synthesized by a vapor-phase transport method. *Crystengcomm* **2015**, *17*, 3214–3218. [[CrossRef](#)]
31. Fjermestad, T.; Svelle, S.; Swang, O. Mechanism of Si Island Formation in SAPO-34. *J. Phys. Chem. C* **2015**, *119*, 2086–2095. [[CrossRef](#)]
32. Dai, W.; Wu, G.; Li, L.; Guan, N.; Hunger, M. Mechanisms of the Deactivation of SAPO-34 Materials with Different Crystal Sizes Applied as MTO Catalysts. *ACS Catal.* **2013**, *3*, 588–596. [[CrossRef](#)]
33. Li, Z.; Martínez-Triguero, J.; Yu, J.; Corma, A. Conversion of methanol to olefins: Stabilization of nanosized SAPO-34 by hydrothermal treatment. *J. Catal.* **2015**, *329*, 379–388. [[CrossRef](#)]

